

Research Paper

Dietary cobalt oxide nanoparticles alleviate aging through activation of mitochondrial UPR in *Caenorhabditis elegans*

Wenshu Cong^{1,2}, Yajie Wang³, Chunhui Yuan², Mei Xu², Han Wang², You Hu², Xuyan Dai⁴, Yuhua Weng¹, Peter Timashev⁵, Xing-Jie Liang⁶, Yuanyu Huang¹✉

1. Advanced Research Institute of Multidisciplinary Science; School of Life Science; School of Medical Technology; Key Laboratory of Molecular Medicine and Biotherapy; Key Laboratory of Medical Molecule Science and Pharmaceutics Engineering; Beijing Institute of Technology, Beijing 100081, P. R. China.
2. Jiangsu Key Laboratory of Brain Disease and Bioinformation, Research Center for Biochemistry and Molecular Biology, Xuzhou Medical University, Xuzhou 221004, P. R. China.
3. Key Laboratory of Combinatorial Biosynthesis and Drug Discovery, Ministry of Education, School of Pharmaceutical Sciences, Wuhan University, Wuhan 430071, P. R. China.
4. Hunan Agricultural University, Changsha 410128, P. R. China.
5. Laboratory of Clinical Smart Nanotechnologies, Institute for Regenerative Medicine, Sechenov University, 119991 Moscow, Russia.
6. CAS Key Laboratory for Biomedical Effects of Nanomaterials and Nanosafety, CAS Center for Excellence in Nanoscience, National Center for Nanoscience and Technology of China, Beijing 100190, P. R. China.

✉ Corresponding author: E-mail: yyhuang@bit.edu.cn (Y.H.).

© The author(s). This is an open access article distributed under the terms of the Creative Commons Attribution License (<https://creativecommons.org/licenses/by/4.0/>). See <http://ivyspring.com/terms> for full terms and conditions.

Received: 2022.12.13; Accepted: 2023.04.21; Published: 2023.05.27

Abstract

Mitochondrial unfolded protein response (UPR^{mt}), which is a mitochondrial proteostasis pathway, orchestrates an adaptive reprogramming for metabolism homeostasis and organismal longevity. Similar to other defense systems, compromised UPR^{mt} is a feature of several age-related diseases. Here we report that dimercapto succinic acid (DMSA)-modified cobalt oxide nanoparticles (Co₃O₄ NPs), which have received wide-spread attention in biomedical fields, is a promising UPR^{mt} activator and, more importantly, provides a gate for extending healthy lifespan.

Methods: UPR^{mt} activation by Co₃O₄ NPs was tested in transgenic *Caenorhabditis elegans* (*C. elegans*) specifically expressing UPR^{mt} reporter Phsp-6::GFP, and the underlying mechanism was further validated by mitochondrial morphology, mtDNA/nDNA, metabolism-related genes' expression, mitonuclear protein imbalance, oxygen assumption and ATP level in *C. elegans*. Then therapeutic response against senescence was monitored by lifespan analysis, lipofuscin contents, MDA contents, Fe accumulation, pharyngeal locomotion performance as well as athletic ability (head thrashes and body bends) at different developmental stages of *C. elegans*. RNAi towards *ubl-5* or *atfs-1* in UPR^{mt} pathway was applied to clarify the role of UPR^{mt} in Co₃O₄ NPs -mediated anti-aging effects. Finally, the effect of Co₃O₄ NPs on mitochondrial homeostasis and D-galactose-induced cell viability decline in mammalian cells were studied.

Results: Co₃O₄ NPs was revealed as a bona fide activator of the UPR^{mt} signaling pathway, through fine-tuning mitochondrial dynamics and inducing a stoichiometric imbalance between OXPHOS subunits encoded by mitochondrial DNA (mtDNA) and nuclear DNA (nDNA) at early life stage of *C. elegans*. Phenotypically, Co₃O₄ NPs treatment protect *C. elegans* from external stresses. More importantly, dietary low level of Co₃O₄ NPs effectively extend lifespan and alleviate aging-related physiological and functional decline of worms, demonstrating its potential roles in delaying aging. While the protective effect exerted by Co₃O₄ NPs was compromised in line with *atfs-1* or *ubl-5* RNAi treatment. Further studies verified the conservation of Co₃O₄ NPs in activating UPR^{mt} and exerting protective effects in mammalian cells.

Conclusions: The results reveal beneficial effects of Co₃O₄ NPs on mitochondrial metabolic control, thus presenting their potential efficacy in anti-aging care.

Keywords: aging, cobalt oxide nanoparticles, *Caenorhabditis elegans*, mitochondrial, unfolded protein response

Introduction

Aging is a main risk factor for diabetes, cancers, cardiovascular diseases and neurodegenerative diseases [1-3]. Currently, the global population of aging individuals is growing intensely, which leads to a worldwide increase in longevity expectancy [4, 5]. One of the main mechanisms underlying compromised physiological function in aging and age-related diseases is cellular stress and damage [1]. Several important protective machineries (i.e., repair and refold machineries and degradation apparatus) have evolved to maintain cellular homeostasis and cope with diverse stresses [6]. When these defense machineries are compromised, as observed in aging and age-related diseases, cell function is misregulated and cell death is accelerated [7-10].

Mitochondrial unfolded protein response (UPR^{mt}) is a master mitochondrial proteostasis pathway orchestrating an adaptive reprogramming of metabolism for the maintenance of cellular homeostasis and cytoprotection [11-16]. Disruption of UPR^{mt} is associated with protein aggregation and is a feature of several age-related diseases [17, 18]. Previous reports have proved it is a conserved longevity mechanism in various animal models and a promising therapeutic target [11-16]. Disturbed balance between OXPHOS subunits encoded by mtDNA and nDNA, a state we termed mitonuclear protein imbalance, is considered as the key route to activate UPR^{mt} [15]. To this end, many genetic approaches, such as constructing loss- or gain-of-function mutations of mitochondrial components, have been adopted to induce mitonuclear protein imbalance and activate UPR^{mt} for alleviating senescence [13, 15]. However, most of these methods show unsatisfactory efficacy with limitations including long-term interference in genes, off-target cleavage, and complex manipulation.

As an essential trace element that generally found in Vitamin B12, cobalt, is critical for the physiological functions and cellular metabolism for animals and human beings [19, 20]. Severe dietary deficiencies of cobalt elements are linked to adverse health effects [21, 22]. Despite the protective effects, traditional cobalt and cobalt compounds have a narrow window between beneficial and toxic effects [23]. Recently, because of multiple advantages such as ease in fabrication, unique bioactivities and low toxicity with acceptable bioavailability, the potential of cobalt based nanoparticles as therapeutic and diagnostic agents has been increasingly investigated [24-26]. For instance, Co₃O₄ NPs were proved with multiple enzyme-like activities in biocatalysis and bioassays [27-29]. Appropriate supplementation of Co^{III} (salen) (acac) was revealed to up-regulate neuroprotective proteins and protect cells from

oxidative stresses [22]. Another study used Co atoms on N-doped carbon as antioxidants to reduce pro-inflammatory cytokine levels and alleviate sepsis [30]. Despite significant progress having been made, the potential effects of Co based nanomaterials on mitochondrial metabolism and the subsequent animal aging process have seldom been explored.

Here, we report that dimercaptosuccinic acid (DMSA) modified cobalt oxide nanoparticles (Co₃O₄ NPs) as a mitochondrial UPR^{mt} activator that alleviates the progression of aging (**Scheme 1**). Because of numerous advantages such as short lifespan, similar metabolism routes as in human, conserved genetic information and signaling pathways [31-33], *C. elegans* were adopted as the model animals to conduct *in vivo* study. We firstly confirmed a dosage window for the application of Co₃O₄ NPs during the therapy. Then we found that Co₃O₄ NPs treatment induce mitonuclear imbalance at the early life stage of worms by influencing fission/fusion and biogenesis/degradation balance, followed by UPR^{mt} activation. More importantly, we demonstrated that Co₃O₄ NPs treatments extend healthy lifespan in *C. elegans* by stimulating UPR^{mt}. Collectively, our results reveal beneficial effects of Co₃O₄ NPs on mitochondrial metabolic control, thus presenting their potential efficacy in anti-aging care.

Results and Discussion

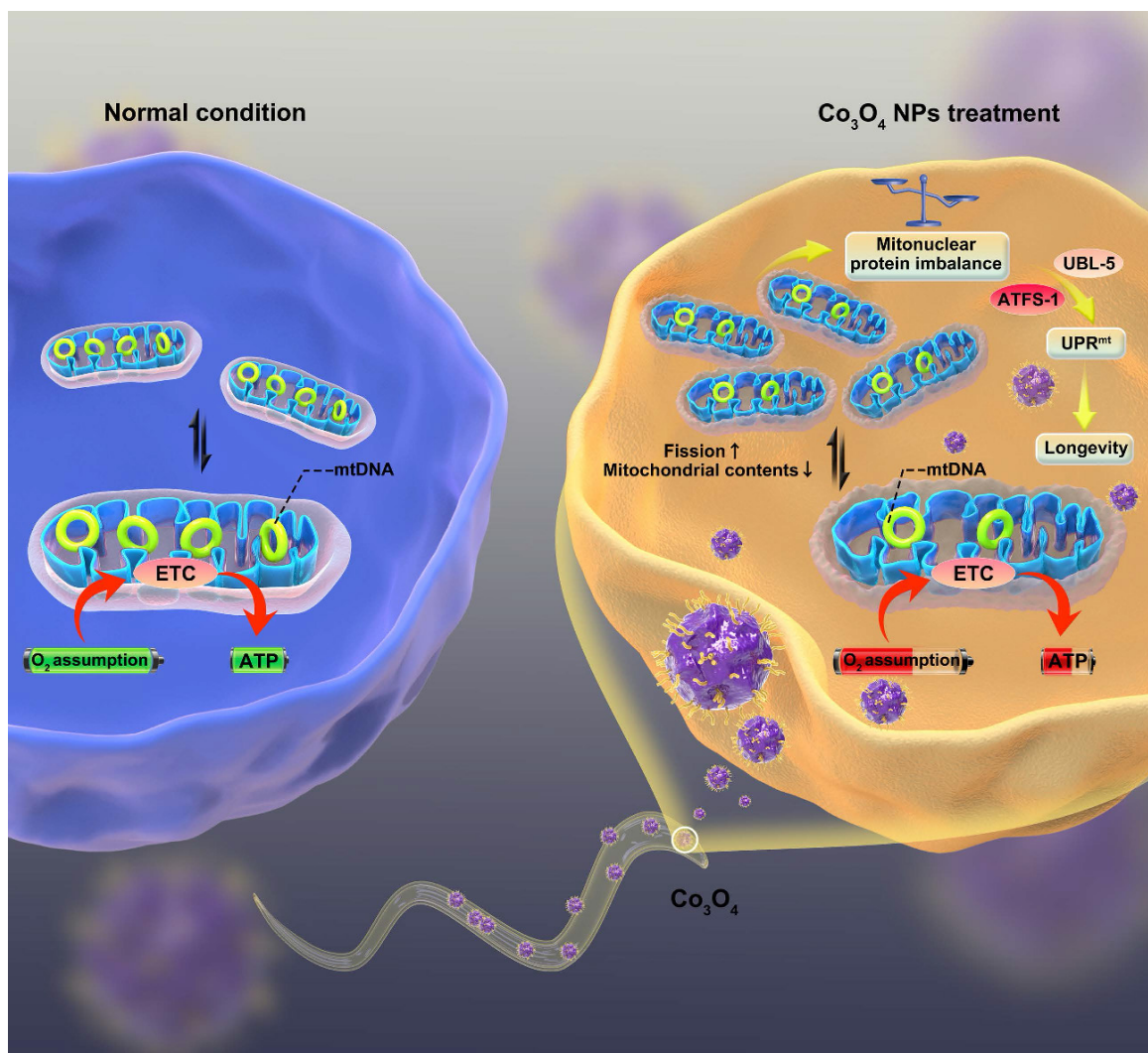
Biocompatibility and Anti-stress Performance Assessment of Co₃O₄ NPs

The Co₃O₄ NPs modified with DMSA used in the study were synthesized by a coprecipitation method as in previous work [26]. We first evaluated the physical properties of Co₃O₄ NPs. As shown by transmission electron microscopy (TEM), the Co₃O₄ NPs were well dispersed and had a uniform spherical shape (**Figure 1A**). The size distributions and zeta potential of the synthesized Co₃O₄ NPs were characterized using dynamic light scattering (DLS), which indicated a uniform size of 200 nm and approximately -17.8 eV (**Figure 1B-C**). Then XRD techniques were employed to analyze the morphology and the phase composition. As shown in **Figure 1D**, all the measured diffraction peaks of the Co₃O₄ NPs XRD pattern matched well to the standard pattern of hausmannite Co₃O₄ NPs, confirming their highly crystalline nature.

To evaluate the biocompatibility of Co₃O₄ NPs, wildtype worms at L1 Larva stage were fed with Co₃O₄ NPs for three days followed by measurements. We found that Co₃O₄ NPs at tested doses (0.005-5 µg mL⁻¹) did not induce any adverse effect on survival rate, body length and egg-laying rate in *C. elegans*

under normal situations (**Figure 1E and Figure S1**). Interestingly, after the exposure to juglone as oxidative stress stimuli, worms pretreated with Co_3O_4 NPs of different concentration at 0.005, 0.05 and $0.5 \mu\text{g mL}^{-1}$ had an increased lifespan, when compared with blank group, suggesting the dosage-dependent protective effect of Co_3O_4 NPs under stress (**Figure 1F**). Since the protective effects of $0.5 \mu\text{g mL}^{-1}$ and $0.05 \mu\text{g mL}^{-1}$ under juglone are similar, Co_3O_4 NPs at $0.05 \mu\text{g mL}^{-1}$ concentrations was adopted for the following studies. We continued to compare the biosafety of Co_3O_4 NPs versus CoCl_2 . Under normal conditions, it was revealed that neither Co_3O_4 NPs nor its inorganic control CoCl_2 induced any adverse effect on larva in terms of pharyngeal pumping rate and body length in worms (**Figure 1G-I**). In addition, Co_3O_4 NPs exposure at $0.05 \mu\text{g mL}^{-1}$ did not induce significant level of reactive oxygen species (ROS) in both cellular and mitochondrial level evaluated by 2',7'-dichloro-

fluorescein diacetate (DCFDA) and Mitosox dyes, correspondingly (**Figure 1J-K and Figure S2**). Whereas CoCl_2 induced ROS to some contents at mitochondrial, reconfirming the superior biosafety of Co_3O_4 NPs compared to its inorganic form (**Figure 1J and Figure S2**). Furthermore, both young and aged worms after treated with Co_3O_4 NPs appeared more resistant under high temperature induced stressed conditions, as the frequency of body bends and head thrashes remained higher than that of the untreated control groups (**Figure 1L-O**). While CoCl_2 did not show any protective effects (**Figure 1L-O**). In conclusion, above findings suggest low levels of Co_3O_4 NPs not only have good biocompatibility, but also demonstrate remarkable protective efficacy to *C. elegans* against external stressors. Furthermore, above results also exclude the possibility of dietary intake restriction due to Co_3O_4 NPs supplementation [34].



Scheme 1. The proposed mechanism by which Co_3O_4 NPs shows anti-aging effect on *C. elegans*.

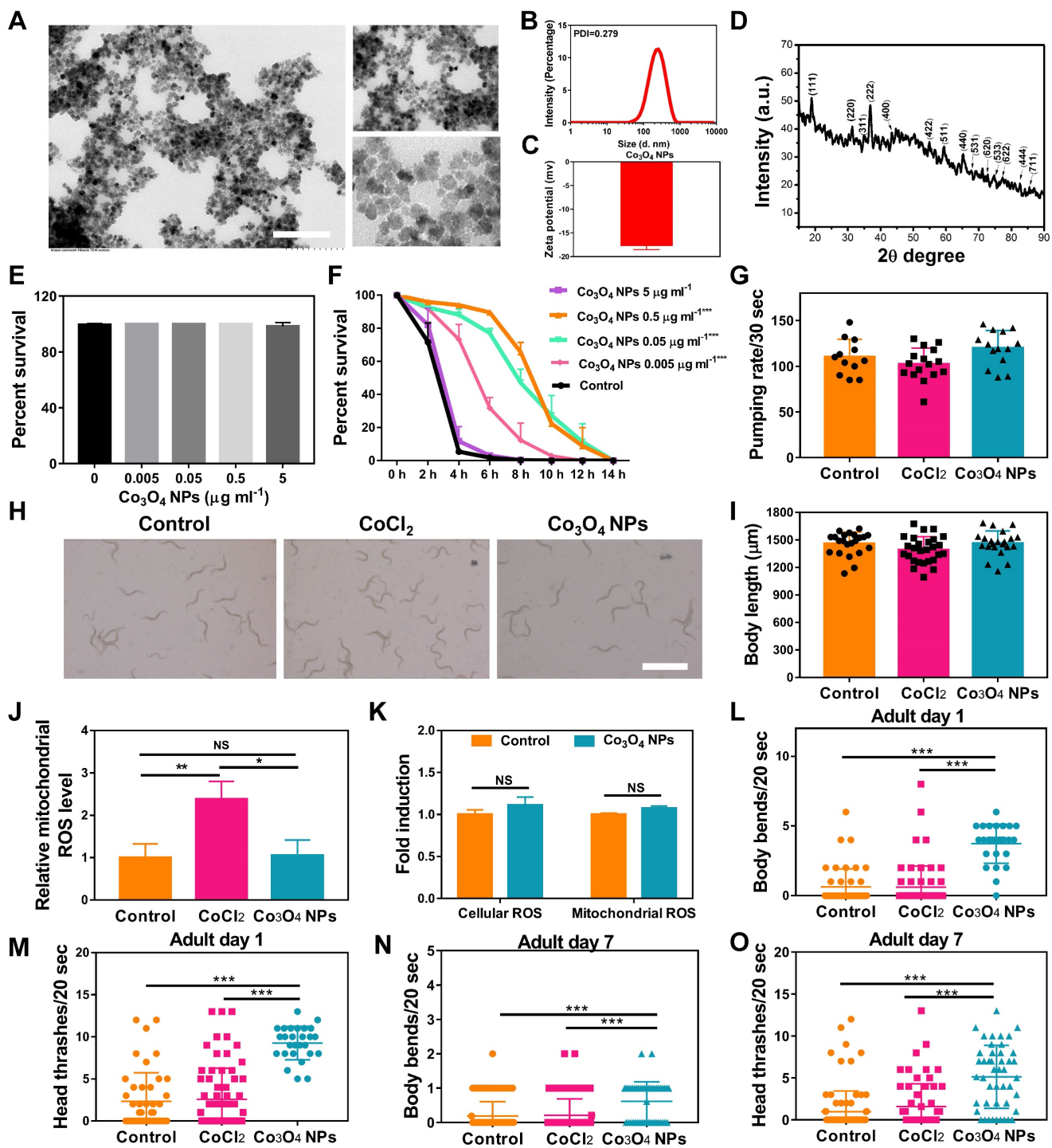


Figure 1. Characterization of physicochemical properties and biocompatibility evaluation of Co_3O_4 NPs. (A) Representative TEM image of Co_3O_4 NPs. Scale bars = 2 μm . DLS histograms (B), zeta potential (C) and powder X-ray diffraction pattern (D) of Co_3O_4 NPs. (E) Lethality of worms treated with gradient doses of Co_3O_4 NPs treatments. (F) Lifespan of worms treated with Co_3O_4 NPs under juglone-induced oxidative stress. Comparison of Co_3O_4 NPs and CoCl_2 at equal doses (0.05 $\mu\text{g mL}^{-1}$) on pumping rate (G) and body length on adult day 1 (H, I). Scale bars = 5 mm. (J) Quantified mitochondrial ROS in *C. elegans* after Co_3O_4 NPs and CoCl_2 treatments. (K) Comparison of mitochondrial and cellular ROS in Co_3O_4 NPs and mock-treated worms on adult day 1. Body bend frequency (L) and head thrash frequency (M) of worms on adulthood day 1 under heat stresses; Body bend frequency (N) and head thrash frequency (O) of worms on adulthood day 7 under heat stresses.

Co_3O_4 NPs Treatment Activates UPR^{mt} Pathway

The unusual protective effects of Co_3O_4 NPs against external stressors inspired us to investigate further. UPR^{mt} is a momentous mitochondrial-to-nuclear stress-signaling pathway that could rewire

the metabolic state and improve immune strength [11-16]. To figure out the beneficial effect exerted by Co_3O_4 NPs, we explored the potential interference of this metabolic sensor by uptake of Co_3O_4 NPs. The worms specifically expressing UPR^{mt} reporter Phsp-6::GFP in the mitochondrial were used for *in*

in vivo monitoring of UPR^{mt} activation after Co₃O₄ treatments. Surprisingly, incubation with Co₃O₄ NPs robustly upregulated the expression of Phsp6::GFP by approximately 60%, while CoCl₂ treatment did not significantly increase GFP signals (Figure 2A-B). Similarly, the endogenous transcriptional level of *hsp-6* had been found to be upregulated in the Co₃O₄ NPs-treated worms (Figure S3). These results confirmed that UPR^{mt} was activated after Co₃O₄ NPs treatment. Ubiquitin-Like Protein-5 (UBL-5) and Activating Transcription Factor-1 (ATFS-1) are the two critical UPR^{mt} regulators that activate mitochondrial chaperones and control mitochondrial transcription, respectively [14, 16, 35]. To further confirm UPR^{mt} activation, we also fed Co₃O₄ NPs to worms with *ubl-5* or *atfs-1* downregulated through RNAi (Figure 2C). As we expected, the upregulation

of Phsp6::GFP activation by Co₃O₄ NPs was abolished in the *ubl-5* or *atfs-1* knockdown worms (Figure 2D-E), supporting the previous findings that identified Co₃O₄ NPs as an activator of the UPR^{mt} pathway.

Additionally, to investigate the role of other pathways involved in stress-resistance paradigm, we also measured the expression of markers of heat shock and ER stress pathways as potential factors for the beneficial effects upon Co₃O₄ NPs exposure. Specifically, Co₃O₄ NPs did not influence transcriptional expression changes of the transcription factor heat shock factor-1 (HSF-1) which regulates the heat shock response (HSR) or heat shock factor-4 (HSF-4) that regulates endoplasmic reticulum (ER) stress when compared with vehicle control group (Figure S4) [36, 37].

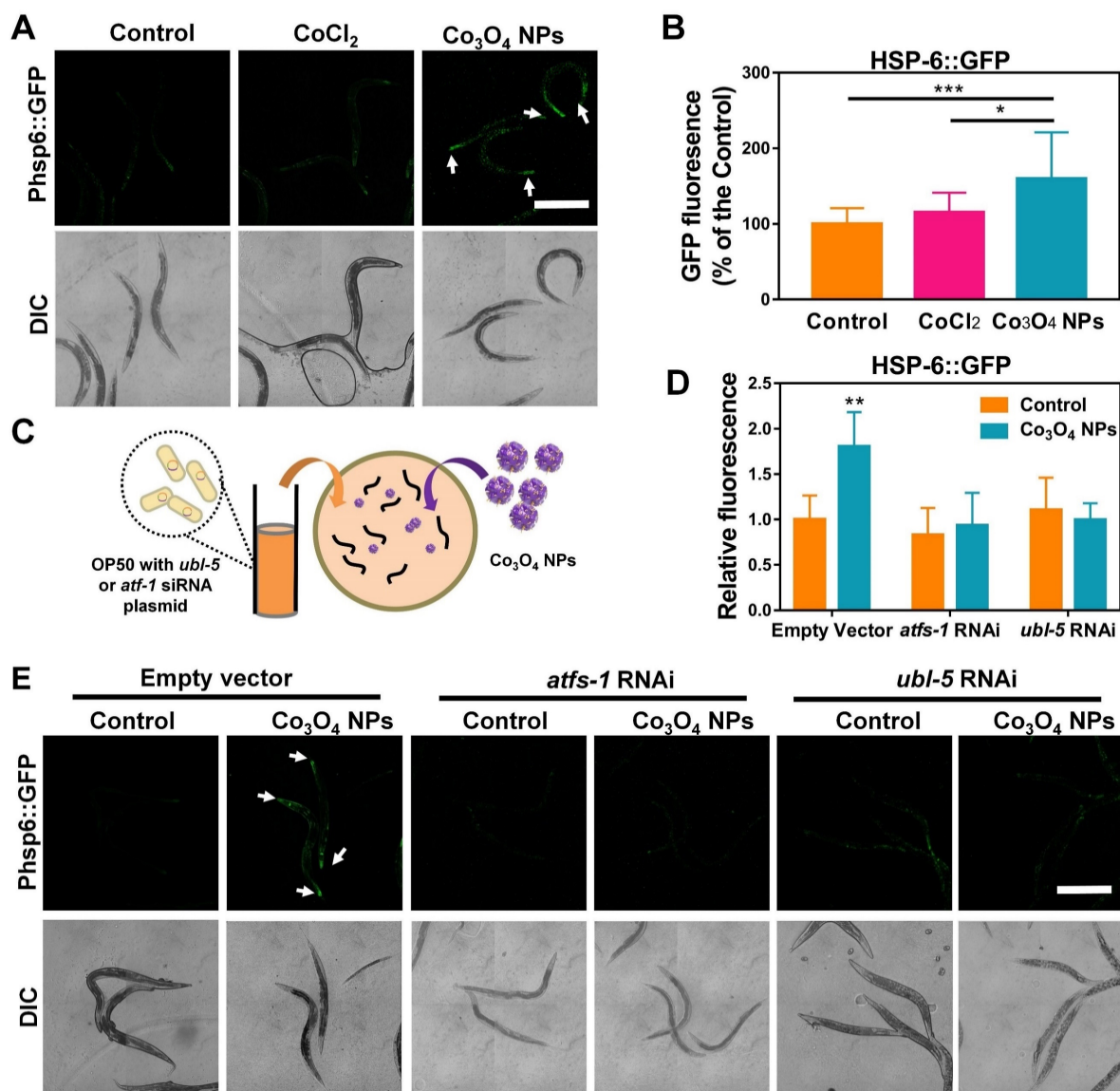


Figure 2. Effect of Co₃O₄ NPs on UPR^{mt} pathway. Fluorescent images (A) and quantification (B) of UPR^{mt} of worms expressing Phsp6::GFP treated with Co₃O₄ NPs, CoCl₂ or not. (C) Schematic diagram of the RNAi test procedures. Quantitative results (D) and representative fluorescent pics (E) of *C. elegans* expressing the UPR^{mt} reporter Phsp6::GFP treated with or without Co₃O₄ NPs, in the presence of control dsRNAs or dsRNAs targeting *ubl-5* or *atfs-1*. DIC: differential interference contrast. Worms were synchronized and treated with Co₃O₄ NPs from L4 stage until the test days. *P < 0.05, **P < 0.01, ***P < 0.001. Scale bar = 0.5 mm.

Co₃O₄ NPs Treatment Mildly Shift Mitochondrial Homeostasis at Early Life Stages

Encouraged by the above results, we continued to identify Co₃O₄ NPs's mode of action on mitochondrial to explore the mechanism for Co₃O₄ NPs induced UPR^{mt} activation. Firstly, transgenic worms expressing mitochondrial-targeted pmyo-3::mito::GFP were used to monitor mitochondrial morphology and contents. It was revealed that the mitochondrial in young worms pretreated with the Co₃O₄ NPs appeared to be more fragmented compared to the regular tubular network in the control or CoCl₂ worms, implying that Co₃O₄ NPs promote mitochondrial fission of worms at young stage (**Figure 3A**). While on adult day 7, mitochondrial fragmentation in Co₃O₄ NPs treated group disappeared, indicating that nematodes gradually adapted to changes in mitochondrial homeostasis caused by Co₃O₄ NPs (**Figure 3A**). Additionally, it was revealed that Co₃O₄ NPs treatment downregulated the transcription of the mitochondrial fusion genes *fzo-1* and *opa-1* in young worms (**Figure 3B**). While on adult day 7, *fzo-1* and *opa-1* expression of Co₃O₄ NPs treated worms became similar or even higher than untreated controls (**Figure 3C**), which were consistent with the morphological changes of nematodes mitochondrial. Above results indicate that Co₃O₄ NPs promote mitochondrial fission at the early life stage, implying the shifted mitochondrial homeostasis caused by Co₃O₄ NPs [38].

Disturbed protein homeostasis in mitochondrial is closely related with UPR^{mt} pathway. Typically, mitochondrial proteins are encoded by both nuclear and mitochondrial genomes. Stoichiometric imbalance between the expression of proteins from these two sources, a state we termed mitonuclear protein imbalance, is the key route to activate the mitochondrial unfolded protein response (UPR^{mt}) [11, 39-41]. To further explore the mechanism by which Co₃O₄ NPs treatment activate UPR^{mt}, we determined whether Co₃O₄ NPs treatment induces mitonuclear protein imbalance. It was found that Co₃O₄ NPs treatment reduced the expression of a set of nuclear genes encoding mitochondrial proteins in young adult worms (**Figure S5A**). Moreover, expression of nuclear contents versus mitochondrial contents in terms of mRNA and protein level were measured. According to the results, Co₃O₄ NPs treatment decreased the mitochondrial DNA (mtDNA)/nuclear DNA (nDNA) ratios, demonstrating its attenuating effect on mitochondrial biogenesis (**Figure 3D** and **Figure S5B**). Correspondingly, a stoichiometric mitonuclear protein imbalance verified by the decreased ratio between the mtDNA-encoded MTCO1 and the

nDNA-encoded ATP5A as oxidative phosphorylation subunits was found in Co₃O₄ NPs treated worms (**Figure 3E**). Together, these data indicated that Co₃O₄ NPs treatments decrease mitochondrial abundance and therefore induce mitonuclear imbalance at the early life stage.

Furthermore, we also set out to verify the functional relevance of decreased mitochondrial abundance. It was revealed that the maximum mitochondrial oxygen consumption of nematodes treated with Co₃O₄ NPs was slighted down-regulated by 23% and 34% compared to the control groups on adult day 1 and day 4, while appeared unaffected on adult day 7 (**Figure 3F** and **Figure S6**). And the basal oxygen consumption of young or aged worms appeared not be affected significantly by Co₃O₄ NPs (**Figure S7**). In accordance with this, the ATP generation in the Co₃O₄ NPs treated nematodes appeared downregulated by about 30% on adult day 1, while became similar to that in the blank control group when worms grew old (**Figure 3G**). Furthermore, the attenuating effect on energy metabolism of Co₃O₄ NPs was also confirmed by gene expression analysis of key metabolic enzymes. It was found that Co₃O₄ NPs treatment downregulated the gene expression of enzymes controlling key metabolic pathways including the glycolysis genes hexokinase (*hvk-1*) and cytochrome C oxidase IV (*cox-4*). While TCA cycle gene citrate synthase-1 (*cts-1*) remained unchanged and gluconeogenesis gene pyruvate carboxylase (*pyc-1*) were slightly up-regulated, implying that Co₃O₄ NPs inhibited carbohydrate catabolism and promoted anabolism in *C. elegans* (**Figure 3H**). Above results demonstrated that Co₃O₄ NPs treatment could mildly interfere mitochondrial activities at early life stage, reconfirming the attenuating efficiency of Co₃O₄ NPs on mitochondrial abundance.

Collectively, by tracking the changes in mitochondrial morphology, contents and activities of nematodes, we deduced that Co₃O₄ NPs activated UPR^{mt} mainly via tuning mitochondrial homeostasis including the fission/fusion and biogenesis/degradation balance, followed by inducing mitonuclear imbalance on early life stage (**Figure 3I**). The metabolic homeostasis seems to be restored along with aging, implying the potential adaptive responses. In a different line, mild decrease in mitochondrial contents and activities on early life stage exerts beneficial effects on lifespan of worms, flies, and mice [16, 42]. Therefore, we speculated that Co₃O₄ NPs' regulatory effects on mitochondrial might contribute to its protective effects.

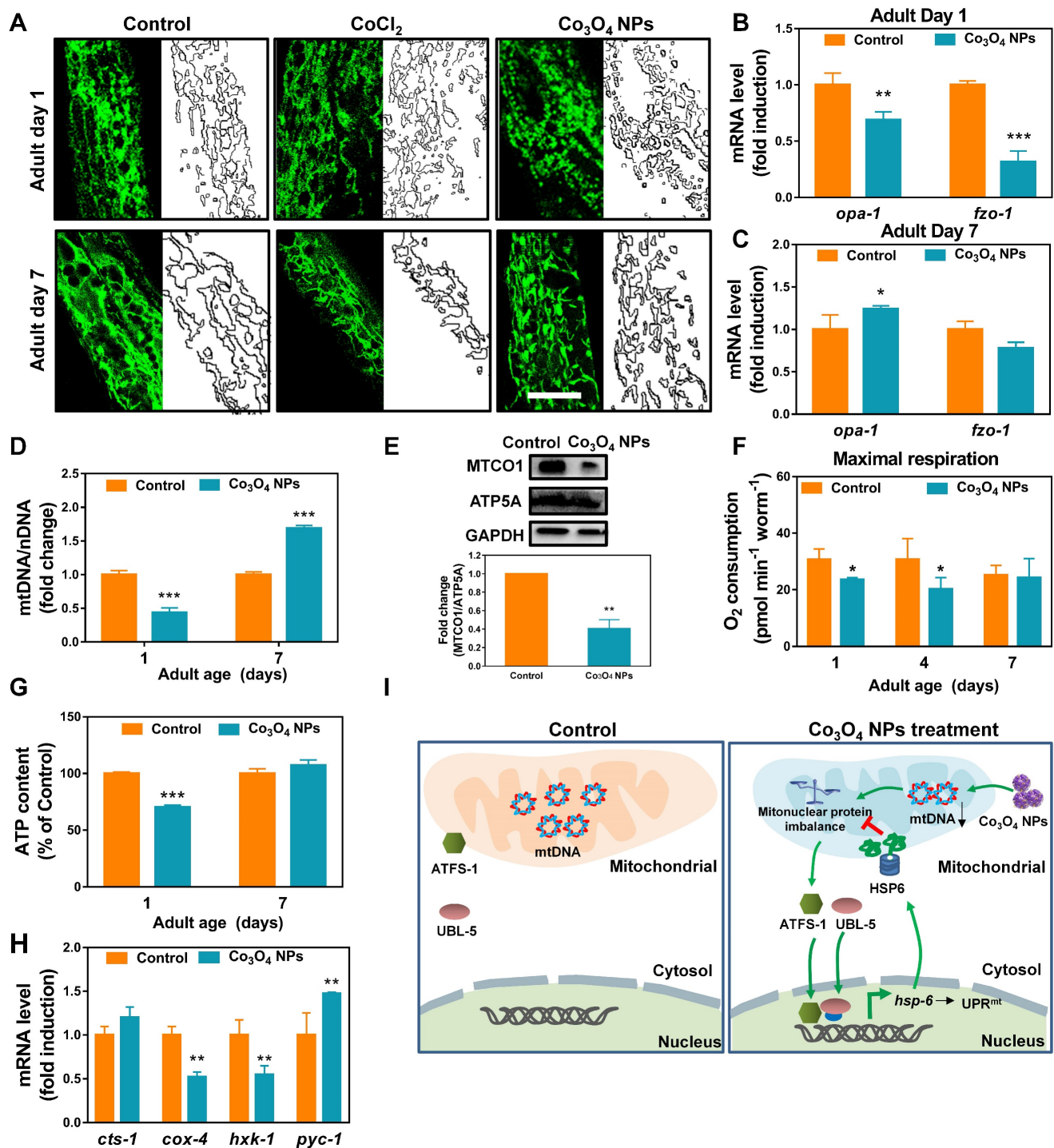


Figure 3. Effect of Co₃O₄ NPs on mitochondrial homeostasis. (A) Representative GFP images of mitochondrial contents on adult day 1 and 7 of worms expressing mitochondrial-targeted *pmyo-3::mito::GFP* reporter in body wall muscle. mRNA expression of mitochondrial fusion genes *fzo-1* and *opa-1* on adult day 1 (B) and adult day 7 (C). (D) Fold change in mtDNA/nDNA ratio (*nd-1/act-3*) on days 1 and 7 of adulthood in worms pretreated with Co₃O₄ NPs or not. (E) Western blot results and quantitative analysis of OXPHOS subunits encoded by nDNA (ATP5A) and mtDNA (MTCO1) in worms. (F) Comparison of maximum oxygen consumption of N₂ worms pretreated with Co₃O₄ NPs or not. (G) Comparison of ATP levels in N₂ worms pretreated with Co₃O₄ NPs or not. (H) Expression of key metabolic genes *cts-1* (TCA cycle), *hxx-1* (glycolysis), *pyc-1* (gluconeogenesis) and *cox-4* (ETC chain enzyme complex IV) in worms on adult days 1. (I) Scheme summarizing how we hypothesize that Co₃O₄ NPs induce activation of UPR^{mt}. The bars represent means ± SD. *P < 0.05, **P < 0.01, ***P < 0.001. Scale bar = 10 μm.

Co₃O₄ NPs Extend *C. elegans* Healthy Lifespan

Because UPR^{mt} plays a key role in innate immunity and pro-longevity machinery in various organisms [11-16], we anticipated an anti-aging role for Co₃O₄ NPs in *C. elegans* as well. We first assessed

the anti-aging propensity of Co₃O₄ NPs by evaluating its efficacy to elongate lifespan of *C. elegans*. Synchronized nematodes were cultured in the medium containing Co₃O₄ NPs at different doses of 0.005-0.5 μg mL⁻¹ (10-fold increase) until death (Figure

4A). As we expected, the worms fed with Co_3O_4 NPs showed longer lifespan in a dose-dependent mode, which was approximately 1.39 times (with $0.005 \mu\text{g mL}^{-1}$ Co_3O_4 NPs), 1.49 times (with $0.05 \mu\text{g mL}^{-1}$ Co_3O_4 NPs), 1.53 times (with $0.5 \mu\text{g mL}^{-1}$ Co_3O_4 NPs) than that of controls, respectively (**Figure 4B** and **Figure S8**). It is noteworthy that dietary Co_3O_4 NPs with UV-killed OP50 bacteria also prolonged the lifespan of *C. elegans* (**Figure S9A**). Additionally, Co_3O_4 NPs at different doses (0.005 – $0.5 \mu\text{g mL}^{-1}$) did not affect the growth rate of OP50 bacteria, ruling out bacterial growth rate alteration as the underlying mechanism for Co_3O_4 NPs-mediated lifespan extension (**Figure S9B**). To further confirm that the extending effect on lifespan was the direct result of Co_3O_4 NPs treatment, we also tested the influence of some other nanoparticles (Fe_2O_3 NPs, Mn_3O_4 NPs and Prussian NPs) on lifespan. None of these nanomaterials at tested concentrations exerted significant effects on elongating worms' lifespan (**Figure S10**). Moreover, the CoCl_2 treatment did not extend lifespan of worms, either (**Figure 4C**), which is speculated due to its failure to activate the UPR^{mt} pathway. Above results implied a unique anti-aging feature of Co_3O_4 NPs.

We further studied the anti-aging potential of Co_3O_4 NPs by monitoring their effects on aging-related biochemical markers and behaviors. Lipofuscin is a non-degradable intralysosomal substance whose accumulation correlates with age and is a useful biomarker for the physiological age of *C. elegans* [43, 44]. As shown in **Figure 4D–E**, the fluorescence intensity in the nematodes treated with Co_3O_4 NPs was less than that of untreated or CoCl_2 NPs-treated controls on both tested days. Of note, compared with the control group, Co_3O_4 NPs-treated aged worms also accumulated lower levels of iron and malondialdehyde (MDA) content, both of which are aging-related markers (**Figure S11**) [45, 46]. Furthermore, the pharyngeal locomotion performance was improved on adult days 6, 9 and 12 when the worms were fed with Co_3O_4 NPs (**Figure 4F**, **Figure S12** and **S13**). We also divided the pharyngeal contractions of worms into three groups: $< 6 \text{ min}^{-1}$ (not pumping), 6 – 147 min^{-1} (slow pumping), and $>147 \text{ min}^{-1}$ (fast pumping), respectively. It was observed that pumping rates decline in the adult nematodes of the control groups along with aging and the behavioral curves of the defined fast pumping worms and low pumping worms intersected on adult day 7. In contrast, the intersection of the curves was delayed until adult day 9 in Co_3O_4 NPs group since the fast pumping rate declined more slowly (**Figure S14**). Similar beneficial effects of Co_3O_4 NPs on athletic ability indicated by head thrashes and body bends were also observed. As shown in **Figure 4G–H**, both

head thrashes and body bend frequencies were robustly improved by the Co_3O_4 NPs treatment along with aging. Altogether, these data demonstrate the outstanding effects of Co_3O_4 NPs on attenuating aging-related behavioral and functional deterioration of *C. elegans*.

Co_3O_4 NPs' Extension of Healthy Lifespan in *C. elegans* is UPR^{mt} Dependent

To further understand the role of UPR^{mt} in Co_3O_4 NPs -mediated anti-aging effects, we studied the lifespan of mutants with loss-of-function in *ubl-5*, *atfs-1* or *dve-1*, all of which are critical regulators in UPR^{mt} pathway [14, 16, 35]. As we expected, attenuating UPR^{mt} by downregulating *ubl-5* or *atfs-1* prevented the lifespan extension induced by Co_3O_4 NPs (**Figure 5A**). Supplementation of Co_3O_4 NPs does not extend lifespan in the *dve-1* (*fx0259*) mutant, either (**Figure S15**). Above observations highlight the importance of UPR^{mt} pathway on the anti-aging efficiency of Co_3O_4 NPs. To further confirm that the anti-aging potential was the direct result of UPR^{mt} activation induced by Co_3O_4 NPs treatment, we also measured the effect of Co_3O_4 NPs on pharyngeal pumping rate in *ubl-5* siRNA, *atfs-1* siRNA or empty vector treated populations. The parameters showed upregulated pharyngeal pumping rate by Co_3O_4 NPs treatment was compromised completely or partly in line with *atfs-1* or *ubl-5* RNAi treatment, respectively (**Figure 5B**). Based on above data, we concluded that Co_3O_4 NPs promoted longevity and improved aging-related behaviors in *C. elegans* mainly through the activation of UPR^{mt}.

Co_3O_4 NPs Treatment Induces UPR^{mt} in Mammalian Cells and Protects Cells from D-galactose-induced Cell Viability Decline

Furthermore, we aimed to investigate Co_3O_4 NPs' influence on mitochondrial homeostasis and their protective roles in mammalian cells. Similar with the findings in *C. elegans*, transmission electron microscopy (TEM) analysis of mitochondrial in human embryonic kidney cells (HEK293T) revealed that Co_3O_4 NPs treatment promotes cellular mitochondrial fission (**Figure S16A**). Noticeably, mitochondrial fission was also accompanied by compromised mitochondrial biogenesis. Co_3O_4 NPs treatment reduced the mtDNA/nDNA ratio (**Figure S16B**), a common marker of mitochondrial abundance in the HEK293T cell line. It was also found that Co_3O_4 NPs treatment downregulated the transcriptional expression of a set of mitochondrial proteins in a dose-dependent mode (**Figure S16C**). Consequently, Co_3O_4 NPs supplement dose-dependently triggers mitonuclear protein imbalance, reflected by decreased

ratio between mtDNA-encoded MTCO1 versus nDNA-encoded SDHA or ATP5A (Figure S16D-F). Furthermore, we also demonstrated that the effects of Co₃O₄ NPs on UPR^{mt} activation are not unique to *C. elegans*. As shown in Figure S16D and Figure S16G, Co₃O₄ NPs induced the UPR^{mt} protease CLPP at the protein level [47]. Consistently, the expression of *hsp60*—the mammalian ortholog of worm *hsp-6*—increased in Co₃O₄ NPs treated HEK293T cells (Figure S16H). Altogether, these data validate the conservation of the UPR^{mt} signaling pathway induced by Co₃O₄ NPs in mammalian cells, as well as the role of

mitonuclear protein imbalance therein. Considering the importance of UPR^{mt} in longevity and cellular protection, we next tested the protective efficiency of Co₃O₄ NPs in D-galactose-accelerated aging cell models [48]. According to CCK8 assay results, the viability of cells exposed to D-galactose was significantly lower than that in blank control group (Figure S16I). In contrast, Co₃O₄ NPs pretreatment partially reversed D-galactose induced cell viability decline (Figure S16I). Altogether, above results indicate the potential of Co₃O₄ NPs as UPR^{mt} activator in mammalian systems for anti-aging therapy.

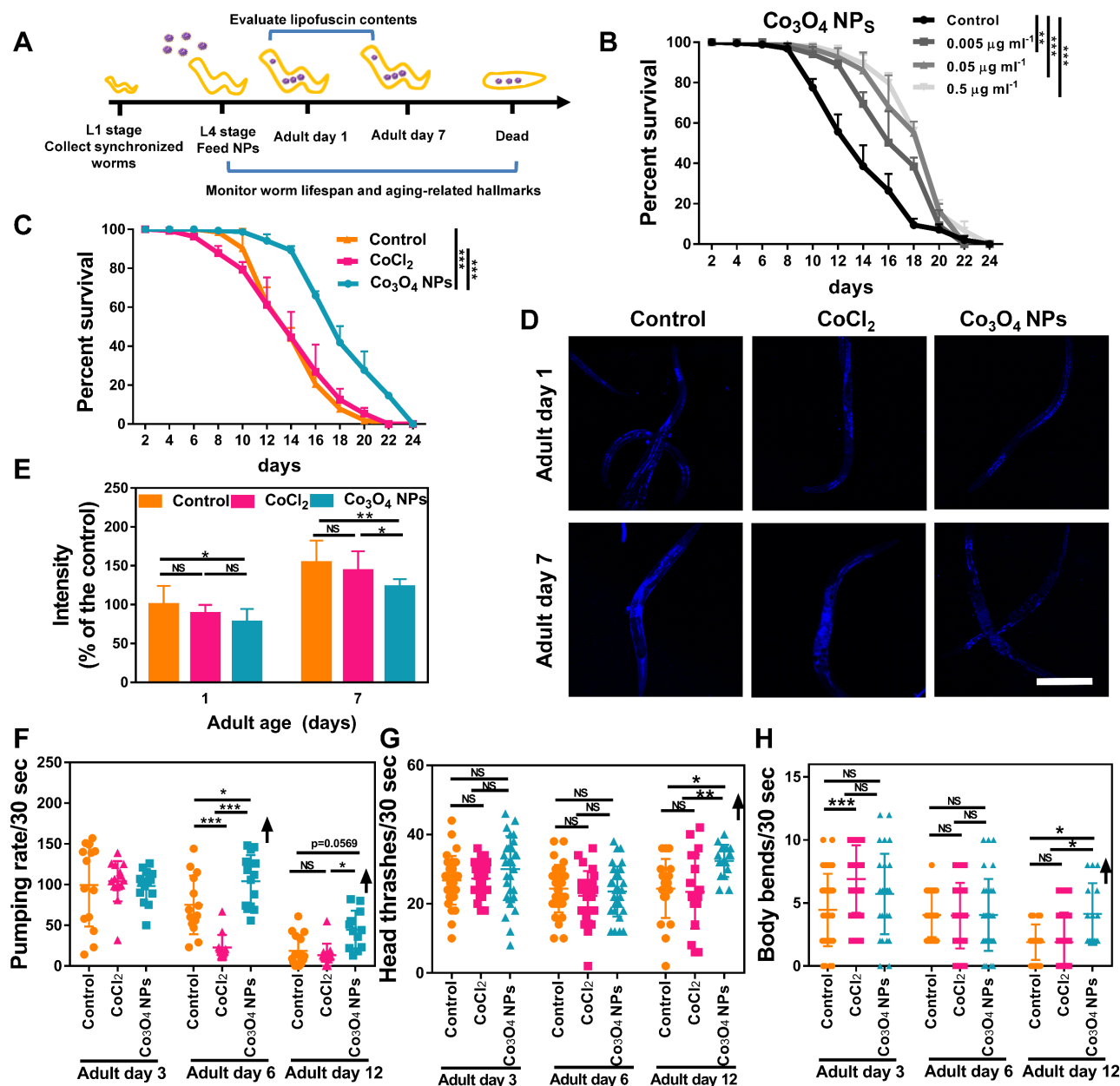


Figure 4. Co₃O₄ NPs extend lifespan and delay age-related behavioral decline in *C. elegans*. (A) Schematic diagram of the anti-aging experimental procedure. Synchronous *C. elegans* populations were collected and treated with Co₃O₄ NPs from the L4 stage until further tests. (B) Lifespan curves of worms in the presence of Co₃O₄ NPs at gradient concentrations. (C) Lifespan curves of worms in the presence of Co₃O₄ NPs, CoCl₂ or not. Average lifespan of control group: 15.1 ± 0.7 days; Average lifespan of CoCl₂ group: 14.8 ± 0.5 days; Average lifespan of Co₃O₄ NPs group: 18.6 ± 0.4 days; The representative fluorescence micrographs (D) and average fluorescence intensity (E) of lipofuscin in N₂ worms on days 1 and 7 of adulthood pretreated with Co₃O₄ NPs, CoCl₂ or not. Pumping rate (F), head thrashes (G) and body bends (H) on days 3, 6 and 12 of adulthood N₂ worms pretreated with Co₃O₄ NPs, CoCl₂ or not. *P < 0.05, **P < 0.01, ***P < 0.001. Scale bar = 0.5 mm.

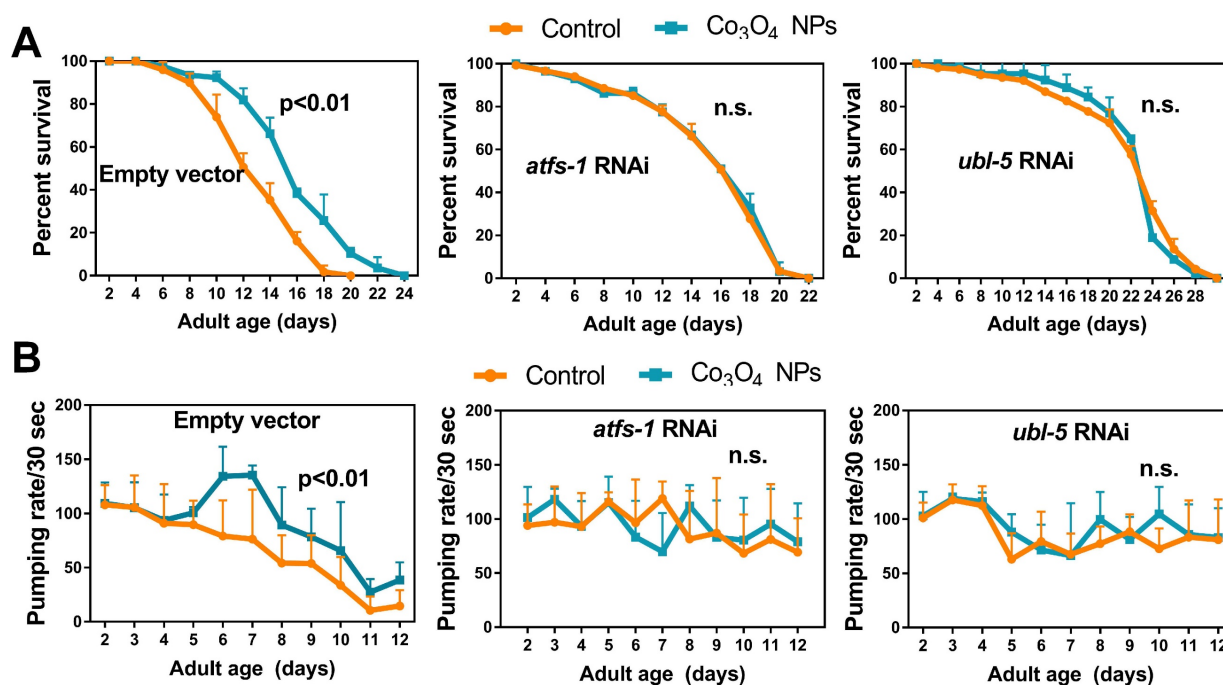


Figure 5. Co_3O_4 NPs confer longevity effects through UPR^{mt} . (A) Lifespan curves of control worms (left), worms treated with *atfs-1* dsRNA (middle) or worms treated with *ubl-5* dsRNAs (right) after Co_3O_4 NPs treatments. (B) Age-dependent decline in pharyngeal pumping of control worms (left), worms treated with *atfs-1* dsRNA (middle) or worms treated with *ubl-5* dsRNAs (right) after Co_3O_4 NPs treatments.

Conclusions

In summary, our study reveals intrinsic anti-aging effects of Co_3O_4 NPs in *C. elegans* models via the activation of the UPR^{mt} signaling pathway. We demonstrate that low levels of Co_3O_4 NPs, under the premise of acceptable compatibility in a whole-animal context, could fine-tune mitochondrial dynamics through increasing mitochondrial fission and inducing mitonuclear imbalance during early developmental age for UPR^{mt} activation. We further validate the anti-aging efficacy of Co_3O_4 NPs in the *C. elegans* model. Oral administration of Co_3O_4 NPs not only extend lifespan but also alleviate aging-related physiological and functional decline. We suggest that activation of UPR^{mt} by Co_3O_4 NPs provides a protective mechanism to shield *C. elegans*, otherwise vulnerable in a compromised environment that elicits aging. Furthermore, our study verifies the conservation of Co_3O_4 NPs' effect in activating UPR^{mt} and providing protection in mammalian cell systems. Taken together, the data suggest that Co_3O_4 NPs can function as a simple and efficient UPR^{mt} activator, laying the foundation for future development of potential cobalt-based nanomedical tools for therapeutics in anti-aging health care treatments.

Methods

Reagents and Strains: $\text{Co}(\text{NO}_3)_2 \cdot 6\text{H}_2\text{O}$ and aqueous ammonia was purchased from Sigma (St. Louis, MO). Dimercapto succinic acid (DMSA) was

provided by Shanghai Lingfeng Chemical Reagent Co. Ltd. The DMSA modified Co_3O_4 NPs were synthesized by a coprecipitation method as previously introduced [27]. In brief, $\text{Co}(\text{NO}_3)_2 \cdot 6\text{H}_2\text{O}$ (0.291 g) and aqueous ammonia (0.81 mL, 25%) were mixed together under stirring at 60 °C (1000 rpm) for 3 h to obtain $[\text{Co}(\text{NH}_3)_6]^{3+}$ solution. The obtained Co_3O_4 precipitates were suspended and mixed with dimercapto succinic acid (DMSA, 0.045 g in 1 mL DMSO) for sonication for 2 h and stirred for 5 h. The precipitates were collected again via centrifugation and washed three times before being dissolved in 50 mL of water. The mixture's pH was adjusted to 9.0–10.0, and then the mixture was sonicated to obtain a stable and clear solution. Finally, the solution was dialyzed in distilled water for 3 days to separate excess DMSA from Co_3O_4 NPs. The Co_3O_4 NPs dispersion was filtered through a 0.22 μm membrane and finally stored at 4 °C for the following studies. Fe_2O_3 NPs, Mn_3O_4 NPs and Prussian blue NPs were purchased from Nanjing Nanoeast Biotech co., LTD. ATP Assay Kit, 2',7'-dichlorodihydrofluorescein diacetate (DCFH-DA) were purchased from Beyotime (Shanghai, China). D-galactose (Cat. No: G5388) was purchased from Sigma-Aldrich (St. Louis, MO). The compound of 5-hydroxy-1,4-naphthoquinone (Juglone, Sigma-Aldrich) was used to induce reactive oxygen species as an oxidative stress generator [49]. Ethanol was adopted as a cosolvent of juglone. 5-fluoro-2-deoxyuridine (FUDR) was used to inhibit nematodes from laying eggs. Cell counting kit 8

(CCK8) assay kit was obtained from Dojindo (Kumamoto, Japan).

C. elegans and Cells Maintenance: Wild-type strains were provided by the Caenorhabditis Genetics Center (University of Minnesota). SJ4100 (zcls13 [HSP-6::GFP]) was a general gift from Professor Caishiing (Institute of Neuroscience and State Key Laboratory of Neuroscience, Chinese Academy of Sciences). Transgenic worms SJ4103 (zcls14 [myo-3::GFP(mit)]) that express mitochondrial-targeted pmyo-3::mito::GFP, as unrestricted gifts from Dr Chen Wenliang (Huainan Normal University), were used to monitor mitochondrial network morphology and contents. PS3551 [hsf-1(sy441)I] and FX0259 (dve-1) mutant worms were generally granted by Professor Xiaochen Wang (Institute of Biophysics, Chinese Academy of Sciences). Unless otherwise specified. The N₂ Bristol strain was used as the reference wild type. *C. elegans* strains were cultured on the nematode growth medium (NGM) at 20 °C and maintained with standard procedures as described previously [50]. Nematodes were obtained by bleaching gravid adults and allowing them to hatch overnight. Synchronized L1 larvae were placed on NGM plates spotted with *Escherichia coli* strain OP50. Upon reaching L4 stage, worms were transferred to NGM plates spotted with OP50, FudR (80 µM) and Co₃O₄ NPs or CoCl₂ at indicated concentrations at 20 °C until further testing or observation. The HEK293T cell line was obtained from the ATCC cell bank and cultured in DMEM medium supplemented with 10% fetal bovine serum. Except otherwise indicated, cells were pretreated with Co₃O₄ NPs or CoCl₂ at 0.05 µg mL⁻¹ for 24 h before further tests.

Characterization of Co₃O₄ NPs: Transmission electron microscopy (TEM) was used to characterize the morphology and size of the Co₃O₄ NPs. The Co₃O₄ NPs solution was dropped onto carbon-coated copper grids and captured for TEM pictures (Jeol 2010, 200KV). Nanosizer ZS90 (Malvern) was leveraged to characterize Dynamic light scattering (DLS) and zeta potential distribution of Co₃O₄ NPs. Moreover, powder X-ray diffraction (XRD) data were collected on a Brucek D8 advance by using Cu Ka radiation. The diffractometer was operated at 40 kV and 40 mA.

Lifespan Test: Synchronized L1 larvae were placed on NGM plates spotted with OP50. Upon reaching L4 stage, approximately 50-100 synchronized L4 stage worms were transferred to NGM placed with OP50, FUDR (80 µM) and tested materials at 20 °C. In all lifespan experiments, worms were scored for live versus dead twice a day by gently tapping worms with a platinum wire. Worms that failed to respond to several taps were scored as dead and removed from the plate. Worms were censored if

they died because of vulval rupture or desiccation from moving off the culture plate.

Body Size Measurements: Synchronized L1 larvae were placed on NGM placed with OP50, 5-FUDR (80 µM) and tested materials at 20 °C. 10-15 worms at indicated developmental age were randomly picked and imaged using a Leica M 165 FC dissecting microscope (Leica). Body size was determined by measuring the length of full body outline using ImageJ software.

Motility Assay: Synchronized L4 stage worms were placed on OP50 plates with FUDR and tested materials at 20 °C until the tested days. Individual nematodes were tracked and 30 s of continuous videos were recorded. The videos were analyzed to calculate worm thrashing number and body bend rate [50, 51]. About 10-15 worms were calculated per group.

Egg-laying rate: A timed egg-lay was performed to synchronize populations. The L1 stages worms were treated with Co₃O₄ NPs (0.005-5 µg mL⁻¹) for three days and collected on adult day 0. After exposure, 30 animals from each exposure group were transferred to new NGM agar plates and allowed to lay eggs for 2 h. Egg-laying rate was defined as the average total number of eggs (10 worms) per hour from the spawning period [52].

Stress Resistance Assay: A timed egg-lay was performed to synchronize populations. The L1 stages worms were treated with Co₃O₄ NPs for three days and collected on adult day 0. For the oxidative sensitivity assay, Co₃O₄ NPs and blank treated worms were seeded on NGM plates with 350 µM juglone and worm viability was monitored every 2 h until death of all worms tested. The number of dead worms was counted by provoking; The heat resistance performance of nematodes was examined [53]. The pretreated worms were incubated at 35 °C for 3 h, followed by being deprived of food at 20 °C for 30 min. Then, the body bends and head thrashes were analyzed according to the procedures introduced above.

Pumping Rate Assay: We counted the contraction number per 30 seconds of the pharyngeal terminal bulb of Co₃O₄ NPs, CoCl₂ or mock-treated worms on an OP50 bacterial lawn under a dissection scope, as described previously [54]. One contraction of the posterior bulb/grind defines one pump. About 10 worms were calculated per group.

Microscopy Analysis: Random number of Co₃O₄ NPs, CoCl₂ or mock-treated worms were placed on 2 % agarose pads and anesthetized with 20 mM NaN₃ before the observation by fluorescence microscopy. To avoid the side effects of NaN₃ on autophagy, all worm slides were freshly constructed and imaged within 15

min. Lipofuscin fluorescence images (excitation: 365 nm; emission: 420 nm) of the worms were captured densitometrically. For the strain SJ4103 (zcls14 [myo-3::GFP(mit)]), the body region was captured using 63×CONFOCAL microscopy. Approximately 10–15 animals were captured for each experimental condition. Fiji ImageJ software was used to visualize and analyze the collected pictures.

Cell Electron Microscopy Analysis: HEK293T cells pretreated with or without Co_3O_4 NPs for 24 h as mentioned above were collected according to manufacturer's procedure. Electron microscopy was used to examine the ultrastructure of mitochondrial morphology.

RNA Interference Experiments: RNAi knockdown experiments were performed as previously described [54, 55]. OP50 bacteria with plasmid clones targeting *atfs-1* and *ubl-5* were purchased from Shanghai HEWU Biotechnology Co. LTD. The bacteria were cultured in LB culture medium containing $100 \mu\text{g mL}^{-1}$ carbenicillin overnight. Then the collected OP50 bacteria were placed on NGM plates together with carbenicillin ($25 \mu\text{g mL}^{-1}$), isopropyl β -D-thiogalactopyranoside (IPTG, 1 mM), and 2'-deoxy-5-fluorouridine (FUDR, $80 \mu\text{M}$). The OP50 bacteria carrying the empty vector L4440 were examined as the control group. Approximately 100 synchronized nematodes were placed on RNAi agar plates at the L4 stage, followed by test procedures.

Worm ATP Level Quantification: Worm ATP level quantification was performed according to a previously reported method [53]. Approximately 100 pretreated nematodes on adult day 1 and day 7 were collected and washed three times to remove bacteria. Then resuspended worms were treated with 5 times freeze/thaw cycles (from liquid nitrogen to 40°C) followed by boiling for 20 min. Then the cooled worm pellets were centrifuged at $11,000 \times g$ for 10 min at 4°C . The supernatant was used for protein quantification and ATP quantification using an ATP detection kit (Thermo Fisher, A22066).

Oxygen Consumption Measurement: We leveraged Seahorse XF24 equipment (Seahorse Bioscience) to measure worm oxygen consumption rate (OCR) [56]. Specifically, synchronized worms were pretreated with or without Co_3O_4 NPs on adult day 1, day 4 and day 7. We rinsed the worms off the culturing plates and washed them three times with M9 buffer by gravity separation. Then, the samples were pipetted into wells of 24-well standard Seahorse assay plates ($18 \text{ worms well}^{-1}$), and 0.5 mL M9 buffer was placed into the blank well for oxygen consumption measurement. We set the instrument protocol to enable the mix cycle to 1, the wait cycle to 3, and the measure cycle to 3 min. Basal respiration was

measured for 4 times. Sequentially, $20 \mu\text{M FCCP}$ (Sigma-Aldrich, Cat# C2920) was added and measured for 8 times to account for maximal respiration. Then 40 mM NaN_3 was added and measured for 4 times to account for non-mitochondrial respiration. The OCR value was normalized to the number of worms per well.

ROS Level Detection: The *C. elegans* were pretreated with Co_3O_4 NPs as previously described and collected. For whole-cell ROS quantification, worms were stained with ROS probe DCFH-DA (Molecular Probes, $25 \mu\text{M}$) for 30 min; For mitochondrial ROS quantification, the samples collected by centrifugation were stained by MitoSox solution ($5 \mu\text{M}$) for 20 min. Then the worms were washed for five times using M9 buffer to eliminate the excess reagent and were placed into 96-well plates for measurement. Quantitative analysis was conducted at excitation/emission wavelengths of 485 and 520 nm.

MDA Content Assay: Synchronized L4 stage worms were pretreated with or without $0.05 \mu\text{g mL}^{-1}$ Co_3O_4 NPs as previously described and collected on adult day 7. To remove bacteria outside of the worms, worms were rinsed three times with M9 buffer. Then the nematodes were collected and broken up by sonication for Malondialdehyde (MDA) analysis using commercially available kits (Beyotime Biotechnology, China) according to the manufacturer's instructions. The total protein mass in different was determined by BCA Protein Assay Kit (Beyotime Biotechnology, China).

Iron quantitation: Synchronized L4 stage worms were pretreated with or without $0.05 \mu\text{g mL}^{-1}$ Co_3O_4 NPs as previously described and collected on adult day 7. Then the dry weight of nematodes in each group was recorded before broken up by sonication. Total iron was measured using a 7700 Series (Agilent) inductively coupled plasma mass spectrometry (ICP-MS) as previously reported [57]. Samples were consisted of at least 100 aged worms per replicate for each group.

Bacteria growth rate: To study if Co_3O_4 NPs exert any possible growth inhibitory and anti-proliferative effect on OP50 bacterial, 1–500 dilution cultures of OP50 bacteria was cultured in liquid LB in the presence of different concentrations of Co_3O_4 NPs in 15 mL sterile tubes. Then the OP50 bacteria were grown overnight with shaking at 37°C . Absorbance (OD 595 nm) was measured at different time points using a microplate reader.

Cell viability assessment: Cell viability was determined using a cell counting kit 8 (CCK8) assay. HEK293T cells were seeded in 96-well tissue culture plates at a density of $1 \times 10^4 \text{ L}^{-1}$ overnight. Then cells were treated with $0.05 \mu\text{g mL}^{-1}$ Co_3O_4 NPs in DMEM

for 6 h. After that, cells were cultured in DMEM with 20 g L⁻¹ D-galactose for 48 h to establish cellular aging model [48]. Finally, 100 µL DMEM with 10% CCK8 was added into each well for 45 minutes incubation. The cell viability was determined by measuring optical absorbance at 450 nm. The assay was repeated in twice.

RT-qPCR: Total RNA was isolated from collected *C. elegans* using TRIzol (Invitrogen). DNA was wiped off using RQ1 RNase-Free DNase (Promega #M6101). cDNA was synthesized using the M-MLV Reverse Transcriptase (Invitrogen #28025013). Gene expression levels were determined by real-time PCR using SYBR Green Supermix. For *C. elegans*, the ratio of relative gene expression values for *nd-1* versus *act-3* represents mtDNA per nuclear genome. This was confirmed with a second mitochondrial gene *mtce.26* versus *act-3*. For mammalian HEK293T cells. HK2 was used as endogenous control for nuclear DNA and 16s was used as marker for mitochondrial DNA. All primers used in this study are listed in Table S1. All data were normalized to the control using actin.

Western Blotting: Western blotting analysis were performed with anti-ATP5A (Abcam), anti-MTCO1 (Abcam), anti-CLPP (Proteintech), anti-SDHA (Proteintech) and anti-GAPDH (Santa Cruz Biotechnology) antibodies. For *C. elegans*, synchronous L4 worms were treated with or without Co₃O₄ at 0.05 µg mL⁻¹ and collected on adult day 1; For mammalian HEK293T cells, cells were treated with indicated concentrations of Co₃O₄ NPs for 24 h. Then nematodes or cells were collected in lysis buffer were sonicated and centrifuged to obtain the supernatant. Afterwards, the samples were boiled in SDS sample buffer for 5-10 min, and separated on SDS-polyacrylamide gel electrophoresis (Bio-Rad) by standard western blotting procedure [58].

Statistical Analysis: All statistics were performed using Graph Pad Prism 7 software. The results are presented as mean ± SE. Data were analyzed by one-way- or two-way analysis of variance (ANOVA), followed by Tukey's multiple comparisons posttest or log-rank test. Differences were regarded as statistically significant (*P < 0.05; **P < 0.01; ***P < 0.001).

Abbreviations

UPR^{mt}: mitochondrial unfolded protein response; Co₃O₄ NPs: cobalt oxide nanoparticles; mtDNA: mitochondrial DNA; nDNA: nuclear DNA; *C. elegans*: *Caenorhabditis elegans*; DMSA: dimercaptosuccinic acid; ROS: reactive oxygen species; DCFDA: 2',7'-dichlorofluorescein diacetate; TEM: transmission electron microscopy; DLS: dynamic light scattering; UBL-5: ubiquitin-like protein-5; ATFS-1: activating

transcription factor-1; HSF-1: heat shock factor-1; HSR: heat shock response; HSF-4: heat shock factor-4; ER: endoplasmic reticulum; *hsk-1*: hexokinase-1; *cox-4*: cytochrome *c* oxidase IV; *cts-1*: citrate synthase; *pyc-1*: pyruvate carboxylase-1; 5-FUDR: 5-fluoro-2-deoxyuridine; NGM: nematode growth medium; XRD: x-ray diffraction; IPTG: isopropyl β-d-1-thiogalactopyranoside; OCR: oxygen consumption rate; HEK293T: human embryonic kidney cells; h: hours; CCK8: cell counting kit 8; ICP-MS: inductively coupled plasma mass spectrometry; MDA: malondialdehyde.

Supplementary Material

Supplementary figures and table.

<https://www.thno.org/v13p3276s1.pdf>

Acknowledgements

This work was supported by the National Key R&D Program of China (2021YFA1201000, 2021YFC2302400, 2021YFE0106900), the Beijing Natural Science Foundation (7214302, 7214283), the Beijing Nova Program from Beijing Municipal Science & Technology Commission (Z201100006820005), and the Fundamental Research Funds for the Central Universities (2022CX01013). We thank the Biological and Medical Engineering Core Facilities, and Analysis & Testing Center, Beijing Institute of Technology for supporting experimental equipment and staffs for valuable help with technical support. We also thank Shiqing Cai from Chinese Academy of Sciences, Xiaochen Wang from Chinese Academy of Sciences and Wenliang Chen from Huainan Normal University for providing transgenic *C. elegans*.

Competing Interests

W.C. and Y.H. are inventors on a patent application related to this work. The other authors have declared that no competing interest exists.

References

- Liguori I, Russo G, Curcio F, Bulli G, Aran L, Della-Morte D, et al. Oxidative stress, aging, and diseases. *Clin Interv Aging*. 2018; 13: 757-72.
- Scott AJ, Ellison M, Sinclair DA. The economic value of targeting aging. *Nat Aging*. 2021; 1: 616-23.
- Lee SS, Lee RY, Fraser AG, Kamath RS, Ahringer J, Ruvkun G. A systematic RNAi screen identifies a critical role for mitochondria in *C. elegans* longevity. *Nat Genet*. 2003; 33: 40-8.
- Mkrtchyan GV, Abdelmohsen K, Andreux P, Bagdonaitis I, Barzilai N, Brunak S, et al. ARDD 2020: from aging mechanisms to interventions. *Aging*. 2020; 12: 24484-503.
- Schmeer C, Kretz A, Wengerodt D, Stojilkovic M, Witte OW. Dissecting Aging and Senescence-Current Concepts and Open Lessons. *Cells*. 2019; 8: 1446.
- Li W, He P, Huang Y, Li Y-F, Lu J, Li M, et al. Selective autophagy of intracellular organelles: recent research advances. *Theranostics*. 2021; 11: 222-56.
- Fiorese CJ, Haynes CM. Integrating the UPR^{mt} into the mitochondrial maintenance network. *Crit Rev Biochem Mol Biol*. 2017; 52: 304-13.
- Douglas PM, Dillin A. Protein homeostasis and aging in neurodegeneration. *J Cell Biol*. 2010; 190: 719-29.

9. Vertti-Quintero N, Berger S, Casadevall i Solvas X, Statzer C, Annis J, Ruppen P, et al. Stochastic and Age-Dependent Proteostasis Decline Underlies Heterogeneity in Heat-Shock Response Dynamics. *Small*. 2021; 17: 2102145.
10. Romeo-Guitart D, Marcos-Dejuana C, Marmolejo-Martinez-Artesero S, Navarro X, Casas C. Novel neuroprotective therapy with NeuroHeal by autophagy induction for damaged neonatal motoneurons. *Theranostics*. 2020; 10: 5154-68.
11. Tian Y, Garcia G, Bian Q, Steffen KK, Joe L, Wolff S, et al. Mitochondrial Stress Induces Chromatin Reorganization to Promote Longevity and UPR(mt). *Cell*. 2016; 165: 1197-208.
12. Shpilka T, Haynes CM. The mitochondrial UPR: mechanisms, physiological functions and implications in ageing. *Nat Rev Mol Cell Biol*. 2018; 19: 109-20.
13. Durieux J, Wolff S, Dillin A. The Cell-Non-Autonomous Nature of Electron Transport Chain-Mediated Longevity. *Cell*. 2011; 144: 79-91.
14. Mouchiroud L, Houtkooper RH, Moullan N, Katsyuba E, Ryu D, Canto C, et al. The NAD(+)/Sirtuin Pathway Modulates Longevity through Activation of Mitochondrial UPR and FOXO Signaling. *Cell*. 2013; 154: 430-41.
15. Houtkooper RH, Mouchiroud L, Ryu D, Moullan N, Katsyuba E, Knott G, et al. Mitonuclear protein imbalance as a conserved longevity mechanism. *Nature*. 2013; 497: 451-7.
16. Campos JC, Wu Z, Rudich PD, Soo SK, Mistry M, Ferreira JC, et al. Mild mitochondrial impairment enhances innate immunity and longevity through ATFS-1 and p38 signaling. *EMBO Rep*. 2021; 22: e52964.
17. Kikis EA, Gidalevitz T, Morimoto RI. Protein homeostasis in models of aging and age-related conformational disease. *Adv Exp Med Biol*. 2010; 694: 138-59.
18. Haynes CM, Ron D. The mitochondrial UPR-protecting organelle protein homeostasis. *J Cell Sci*. 2010; 123: 3849-55.
19. Miles LM, Mills K, Clarke R, Dangour AD. Is there an association of vitamin B12 status with neurological function in older people? A systematic review. *Br J Nutr*. 2015; 114: 503-8.
20. Schaffner A, Li X, Gomez-Llorente Y, Leandrou E, Memou A, Clemente N, et al. Vitamin B12 modulates Parkinson's disease LRRK2 kinase activity through allosteric regulation and confers neuroprotection. *Cell Res*. 2019; 29: 313-29.
21. Ames BN. Prolonging healthy aging: longevity vitamins and proteins. *Proc Natl Acad Sci*. 2018; 115: 10836-44.
22. Schieber C, Howitt J, Putz U, White JM, Parish CL, Donnelly PS, et al. Cellular up-regulation of Nedd4 family interacting protein 1 (Ndfip1) using low levels of bioactive cobalt complexes. *J Biol Chem*. 2011; 286: 8555-64.
23. Leyssens L, Vinck B, Van Der Straeten C, Wuyts F, Maes L. Cobalt toxicity in humans-A review of the potential sources and systemic health effects. *Toxicology*. 2017; 387: 43-56.
24. Novak S, Drobne D, Golobic' M, Zupanc J, Romih T, Gianoncelli A, et al. Cellular internalization of dissolved cobalt ions from ingested CoFe₂O₄ nanoparticles: *in vivo* experimental evidence. *Environ Sci Technol*. 2013; 47: 5400-8.
25. Zhao Y, Zhang Z, Pan Z, Liu Y. Advanced bioactive nanomaterials for biomedical applications. *Exploration*. 2021; 1: 20210089.
26. Hou MM, Zhong YX, Zhang L, Xu ZG, Kang YJ, Xue P. Polydopamine (PDA)-activated cobalt sulfide nanospheres responsive to tumor microenvironment (TME) for chemotherapeutic-enhanced photothermal therapy. *Chin Chem Lett*. 2021; 32: 1055-60.
27. Dong J, Song L, Yin JJ, He W, Wu Y, Gu N, et al. Co₃O₄ nanoparticles with multi-enzyme activities and their application in immunohistochemical assay. *ACS Appl Mater Interfaces*. 2014; 6: 1959-70.
28. Waris A, Din M, Ali A, Afridi S, Baset A, Khan AU, et al. Green fabrication of Co and Co₃O₄ nanoparticles and their biomedical applications: A review. *Open Life Sci*. 2021; 16: 14-30.
29. Ghasemzadeh MA, Abdollahi-Basir MH, Elyasi Z. Synthesis of some Novel Imidazoles Catalyzed by Co₃O₄ Nanoparticles and Evaluation of their Antibacterial Activities. *Comb Chem High Throughput Screen*. 2018; 21: 271-80.
30. Cao F, Zhang L, You Y, Zheng L, Ren J, Qu X. An Enzyme-Mimicking Single-Atom Catalyst as an Efficient Multiple Reactive Oxygen and Nitrogen Species Scavenger for Sepsis Management. *Angew Chem Int Ed Engl*. 2020; 59: 5108-15.
31. Yanase S, Ishii T, Yasuda K, Ishii N. Metabolic Biomarkers in Nematode *C. elegans* During Aging. *Adv Exp Med Biol*. 2019; 1134: 163-75.
32. Denzel MS, Lapierre LR, Mack HHD. Emerging topics in *C. elegans* aging research: Transcriptional regulation, stress response and epigenetics. *Mech Ageing Dev*. 2019; 177: 4-21.
33. Douglas AE. Simple animal models for microbiome research. *Nat Rev Microbiol*. 2019; 17: 764-75.
34. Tain LS, Lozano E, Sáez AG, Leroi AM. Dietary regulation of hypodermal ployploidization in *C. elegans*. *BMC Dev Biol*. 2008; 8: 28.
35. Benedetti C, Haynes CM, Yang Y, Harding HP, Ron D. Ubiquitin-like protein 5 positively regulates chaperone gene expression in the mitochondrial unfolded protein response. *Genetics*. 2006; 174: 229-39.
36. Uddin MS, Yu WS, Lim LW. Exploring ER stress response in cellular aging and neuroinflammation in Alzheimer's disease. *Ageing Res Rev*. 2021; 70: 101417.
37. Kruta M, Sunshine MJ, Chua BA, Fu Y, Chawla A, Dillingham CH, et al. Hsf1 promotes hematopoietic stem cell fitness and proteostasis in response to *ex vivo* culture stress and aging. *Cell stem cell*. 2021; 28: 1950-65.e6.
38. Detmer SA, Chan DC. Functions and dysfunctions of mitochondrial dynamics. *Nat Rev Mol Cell Biol*. 2007; 8: 870-9.
39. Palikaras K, Lionaki E, Tavernarakis N. Coordination of mitophagy and mitochondrial biogenesis during ageing in *C. elegans*. *Nature*. 2015; 521: 525-8.
40. Melber A, Haynes CM. UPR^{mt} regulation and output: a stress response mediated by mitochondrial-nuclear communication. *Cell Res*. 2018; 28: 281-95.
41. Zhu D, Li X, Tian Y. Mitochondrial-to-nuclear communication in aging: an epigenetic perspective. *Trends Biochem Sci*. 2022; 47: 645-59.
42. Zhu D, Wu X, Zhou J, Li X, Tian Y. NuRD mediates mitochondrial stress-induced longevity via chromatin remodeling in response to acetyl-CoA level. *Sci Adv*. 2020; 6: eabb2529.
43. Son HG, Altintas O, Kim EJE, Kwon S, Lee SV. Age-dependent changes and biomarkers of aging in *Caenorhabditis elegans*. *Ageing Cell*. 2019; 18: e12853.
44. Moreno-García A, Kun A, Calero O, Medina M, Calero M. An overview of the role of lipofuscin in age-related neurodegeneration. *Front Neurosci*. 2018; 12: 464.
45. Jenkins NL, James SA, Salim A, Sumardy F, Speed TP, Conrad M, et al. Changes in ferrous iron and glutathione promote ferroptosis and frailty in aging *Caenorhabditis elegans*. *Elife*. 2020; 9: e56580.
46. Angelova PR, Barilani M, Lovejoy C, Dossena M, Viganò M, Seresini A, et al. Mitochondrial dysfunction in Parkinsonian mesenchymal stem cells impairs differentiation. *Redox Biol*. 2018; 14: 474-84.
47. Haynes CM, Petrova K, Benedetti C, Yang Y, Ron D. ClpP mediates activation of a mitochondrial unfolded protein response in *C. elegans*. *Dev Cell*. 2007; 13: 467-80.
48. Azman KF, Zakaria R. D-Galactose-induced accelerated aging model: an overview. *Biogerontology*. 2019; 20: 763-82.
49. Ahmad T, Suzuki YJ. Juglone in oxidative stress and cell signaling. *Antioxidants*. 2019; 8: 91.
50. Cong W, Wang P, Qu Y, Tang J, Bai R, Zhao Y, et al. Evaluation of the influence of fullerene on aging and stress resistance using *Caenorhabditis elegans*. *Biomaterials*. 2015; 42: 78-86.
51. Han B, Sivaramakrishnan P, Lin CJ, Neve IAA, He J, Tay LWR, et al. Microbial Genetic Composition Tunes Host Longevity. *Cell*. 2018; 173: 1058.
52. Li J, Qu M, Wang M, Yue Y, Chen Z, Liu R, et al. Reproductive toxicity and underlying mechanisms of di (2-ethylhexyl) phthalate in nematode *Caenorhabditis elegans*. *J Environ Sci*. 2021; 105: 1-10.
53. Yuan J, Chang SY, Yin SG, Liu ZY, Cheng X, Liu XJ, et al. Two conserved epigenetic regulators prevent healthy ageing. *Nature*. 2020; 579: 118-22.
54. Yin JA, Gao G, Liu XJ, Hao ZQ, Li K, Kang XL, et al. Genetic variation in glia-neuron signalling modulates ageing rate. *Nature*. 2017; 551: 198-203.
55. Kamath RS, Martinez-Campos M, Zipperlen P, Fraser AG, Ahringer J. Effectiveness of specific RNA-mediated interference through ingested double-stranded RNA in *Caenorhabditis elegans*. *Genome Biol*. 2001; 2: Research0002.
56. Koopman M, Michels H, Dancy BM, Kamble R, Mouchiroud L, Auwerx J, et al. A screening-based platform for the assessment of cellular respiration in *Caenorhabditis elegans*. *Nat Protoc*. 2016; 11: 1798-816.
57. James SA, Roberts BR, Hare DJ, de Jonge MD, Birchall IE, Jenkins NL, et al. Direct *in vivo* imaging of ferrous iron dyshomeostasis in ageing *Caenorhabditis elegans*. *Chem Sci*. 2015; 6: 2952-62.
58. Zhang MJ, Shao WX, Yang TR, Liu HL, Guo S, Zhao DY, et al. Conscripton of immune cells by light-activatable silencing NK-derived exosome (LASNEO) for synergetic tumor eradication. *Adv Sci*. 2022; 9: 2201135.